Chaos, Solitons and Fractals 153 (2021) 111396

Contents lists available at ScienceDirect

Chaos, Solitons and Fractals

Nonlinear Science, and Nonequilibrium and Complex Phenomena

journal homepage: www.elsevier.com/locate/chaos

Fractal moiré interferometry

Zbigniew Motyka

Central Mining Institute, Plac Gwarków 1, 40-166 Katowice, Poland

ARTICLE INFO

Article history:
Received 12 February 2021
Revised 17 August 2021
Accepted 23 August 2021
Available online 29 October 2021

Keywords:
Cantor sets
Fractals
Moiré fringes
Moiré interferometry
Gratings
Strains
Displacements

ABSTRACT

Fractal geometry of 2D gratings, based on a regular class of generalized Cantor sets, was proposed to derive moiré fringes with geometry induced by the fractal geometry of these gratings. The general case of a regular fractal grating based on parallel lines was considered. Some simple examples based on parallel straight lines of fractal gratings reduced to the first few steps of fractal grating geometry are briefly discussed. The formation of derivative fractal patterns of interference fringes, which at each fractal step meets the general rules for ordinary moiré patterns, is briefly discussed.

1. Introduction

Moiré methods are widely used in engineering to measure such quantities as in-plane displacements, curvatures, out-of-plane displacements, rotations and strains. Geometrical methods of moiré fringe analysis are based on the phenomenon of fringes' interference occurring when two (or more) sets of gratings are superimposed. The examples of such gratings are equally spaced straight lines or concentric equally spaced circles, as well as two orthogonal sets of crossed equally spaced parallel lines or even the dots being the geometrical complementary of the latter [1]. The use of such gratings enables measurements of deformations or strains with accuracy directly related to densities of the grating lines. In this paper, the gratings of fractal geometry suitably modified both for more rough as well as for finer moiré techniques are proposed. For need of this aim, the notion of *fractal grating,* which incorporates many gratings (in a strong sense an infinite number) of finer and finer, stepped pitches will be introduced. It may be shown that some (if not all of them) conventional gratings may be easily transformed into fractal ones and this, in principle, may result in accuracy of measurements increase due to use of the many-level (in practice at least two) fractal gratings at one-shot engineering measurements.

The notion of *fractal grating* is introduced here to stress the specific character of these gratings derived from some regular class of generalized Cantor sets (strictly speaking: generalized Sierpinski carpets), which in principle may be understood as 1D fractals. Such gratings as well as derived from them moiré fringes possess 1D fractal geometry of generalized Cantor set only along the lines perpendicular to the lines of gratings or moiré fringes. These fringes or lines of gratings are simply composed of common geometrical objects, i.e. lines or more precisely speaking strips. It is their spatial distribution and composition what gives them their fractal character.

2. Fringe moiré

For conventional line gratings in moiré interferometry, centre-to-centre distance between the particular grating lines is assumed to be constant and is called a pitch.

For convenience, it will be assumed here that the pitch p_0 (fringe spacing for s lines per unit length) of the conventional line grating is equal to the double width of its lines. One of two gratings necessary to produce moiré fringes is usually bound with (or projected onto) a surface of an object under investigation. Therefore, its pitches depend locally on the deformations of the object's surface, so it is known as the specimen (or model) grating. The other one is called the master (or reference) grating. They are superimposed to obtain the moiré fringe pattern (Fig. 1.). If the object grating is subjected to deformations comparable with its pitch or greater, the deformation (e.g. elongation, contraction or torsion) of the specimen results in variations of the model grating pitch and consequently in occurrence of the distorted picture of moiré fringes.

E-mail address: z_motyka@wp.pl

https://doi.org/10.1016/j.chaos.2021.111396
0960-0779/

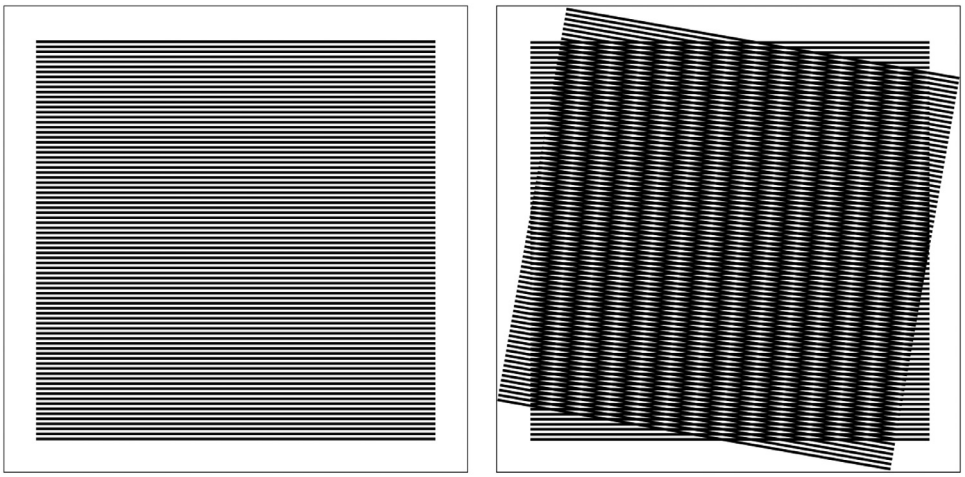

(a) (b)

Fig. 1. An example of linear grating (a) composed of 80 parallel lines and the moiré fringe pattern (b) resulting from superimposing of two such gratings intersecting at the angle 10°.

For example, in measurements of out-of-plane displacements, the shadow moiré method is especially suitable [2]. In this technique a single grating is used as the reference grating and its shadow projection onto the surface of an object under investigation fulfils the role of the specimen grating. While viewing this shadow grating throughout the reference one, one can observe the moiré fringes structure resulting from the surface displacements. When using typical gratings of equally spaced straight lines, the fringes are becoming "denser" (their spatial frequency increases) with the increase of the gradient of such displacement at the direction normal to them.

For better understanding of the meaning and significance of moiré fringe pattern and its parameters, such as the angle of inclination γ and distance w between fringes, we can look once more at Fig. 1. It presents the simplest case of interference in common plane of two gratings with equal pitches p_0 and relative rotation on angle $\beta = 10^\circ$ with respect to each other.

It can be easy seen that

$$w = p_0 \frac{\sin\gamma}{\sin\beta}, \quad where \ \gamma = \frac{\pi - \beta}{2} \tag{1}$$

The angle γ of fringe inclination in relation to lines of one of two superimposed gratings may be easily determined from the symmetry of the problem: moiré fringes lie along the direction of bisector of obtuse angle 2γ between lines of interfering gratings. For $\beta = 10^\circ$ we have $\gamma = 85^\circ$ and $w = 5.7369 p_0$.

The accuracy of the method depends on the pitch of gratings applied. Usually we are restricted to the pitch of earlier prepared gratings and many fine effects cannot be detected with the use of them. Especially, when we are prepared for measurement of rough surface effects only. Usually, it is important to have gratings of the pitch matching the scale of anticipated effect to be measured. Having them, it is easier to proceed with the obtained graphical data. But what to do when the effect becomes whole the rank of magnitude finer during the same measurement process? In such a case we are forced to adopt finer gratings and this is connected with major changes in the measuring setup. It should be noticed that all the above mentioned methods, as well as the one proposed below, allow to measure surface deformations comparable with the pitch of projected gratings. Therefore, they are as a rule especially useful for the measurements of deformations of parts of large and smaller industrial objects, such as tanks, pipes, machines or parts of them. Although, it is worth to recall that the same methods can be used at the sublevels, for which greater accuracy is demanded, as well. The latter is restricted only by the resolution of possible subsequent gratings and recording devices (cameras). On contrary, the proposed here method of fractal moiré allows, in principle, to obtain in one-shot-engineering-measurement a different accuracy, increasing throughout many levels. Of course, the latter have to be adjusted in such a way, which would assure to achieve the balance between the lowest and highest resolution. It is worthy to use such at least two-level solutions for better measurements of surfaces having many-level intrinsically fractal character themselves. It does mean that the accuracy difference shall to be suitably differentiated *a priori*, still. But the range of possible simultaneous measurements extends significantly and this alone seems to be of particular significance. Therefore, there seems to be nothing strange in the fact that fractal structures would prefer the fractal measuring means.

3. Multiple pitch fractal gratings

In the present paper, the possible solution for simultaneous measurements of at least dual resolution is presented. It is based on entirely new proposition of introducing some form of fractal geometry to moiré interferometry methods using at least two different pitches for at least two subsequent sets of strip lines, where each strip line (of finite wideness) itself consists of the set of finer strip lines. All this with typical for fractals pattern at least in one direction in the plane (perpendicular to the direction of lines). As the matter of fact, we will show that also the common gratings (as the one on Fig. 1) may be easily turned into full fractal grating without loss of its course shape and structure at the first glance, at least. It is not yet the case of Fig. 2, thought. Nevertheless, both the figures have many in common with this explanation, as it will become clear soon in the following sections.

To achieve this let us start with its construction. Without significant lost of generalization, we define our grating within a unit square. Let us denote $p_1 = 1/m$ as a pitch of a grating of unit length as well as unit width in the primary direction (the direction perpendicular to its lines), where $m > 0$ is a number of fringes per unit length. Let number m of the lines of the grating be uniformly distributed within unit length in such a way, that the first of them touches the upper boundary of such grating of unit width, form-

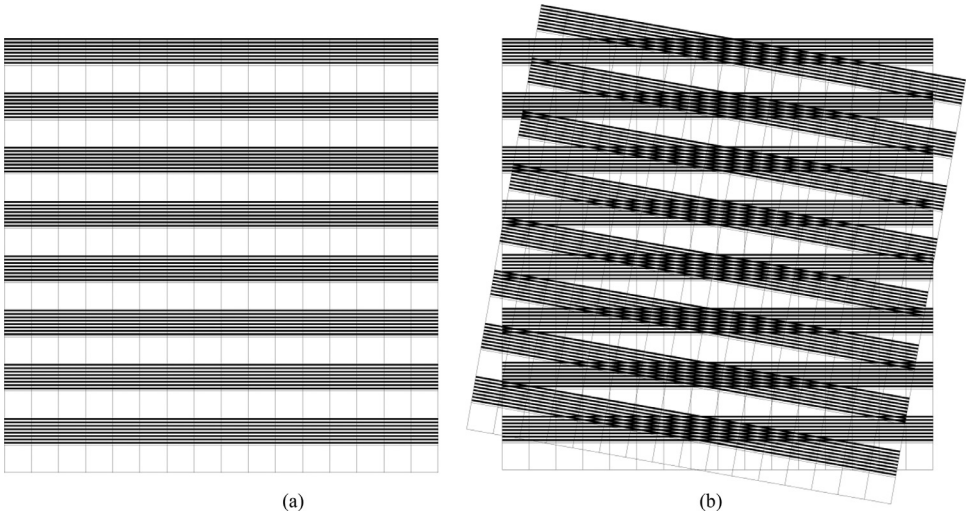

(a) (b)

Fig. 2. (a) An example of fractal grating based on splitting of each grating line into 8 subsequent equally spaced lines. For convenience the constructional subsequent squares are also depicted. They were helpful during the graph construction but are not part of the fractal grating. Assuming that the height of the picture for whole the 8 main lines would be equal to unit length 1 we obtain: the pitch of lower order is equal $p_1 = 1/8$ and the pitch of higher order grating is equal to $p_2 = 1/128$. (b) The moiré fringe pattern resulting from superimposing of two such gratings intersecting at the angle 10°.

ing first order grating with a pitch $p_1 = 1/m$. As a result, we obtain m "dark" strip lines of width $p_1/2$ each, separated with $(m\text{-}1)$ white strips of the same width. The last, m-th white strip is adjacent to the bottom border of the unit square. (And all this within the starting strip of unit length.) Let us take now any "dark" strip line of the first rank grating and subdivide it into another m finer strip lines in a similar way as the initial unit width. In such a way we replace this initial strip line with strip lines of second order grating. Let us do it for all the lines of first order grating. We have obtained two first steps of construction of our fractal grating. An example of such 2-step fractal grating is presented on the left-hand side diagram of the Fig. 2 for $m = 8$. It is based on division of each grating strip line into 8 subsequent equally spaced strip lines. (The number 8, assumed only as an example here, may be replaced with any other natural number $m > 1$.) If the pitch of the lower order grating is equal to $p_1 = 1/m$, then the pitch of the higher order grating (we will name it the *second*-order sub-grating) is equal to $p_2 = 1/(2m^2)$. For the Fig. 2 , for which $m = 8$, $p_1 = 1/8$ and $p_2 = 1/128$. In general, for r-order sub-grating we have $p_r = 1/(2^{r-1}m^r)$. (For convenience, we assumed here that the sub-grating order increases with increase of r.) It can be easily seen that the subsequent grating forms a conventional grating only in the frames of a single strip line of the lower order, leaving left waste blank areas. The right-hand side diagram of Fig. 2 presents an analogue of right-hand side diagram from the Fig. 1, i.e. the moiré fringe pattern resulting from superimposing of two such fractal gratings intersecting at the angle 10°.

There is similar interference pattern present on both the figures, but at the Fig. 2 it is accompanied by the much more coursed, composed of the wider strips of the lower order grating. There may be distinguished two darker strips on the both sides of the one central light. The later is composed of dark and light strips of the higher order sliced with waste blank areas.

This central fringe has in average less grey density then the two darker on both its sides. However, its brighter character is reduced by the dominating at its area number of intersecting points of the higher order lines, resulting with dark fringes of this higher order moiré fringe pattern.

In the following section more rigid construction of three different classes of similar fractal gratings of different m (built of m parallel strip lines at each sub-level) is presented. To achieve this goal, slightly more rigid mathematical formulation based on suitably generalized concept of Cantor set (and suitably generalized regular Sierpinsky carpet) is discussed.

4. An application of cantor sets to fractal gratings

Consider the regular subclass of generalized Cantor sets, generated by subdividing unit length $I = [0,1]$ on k equal segments and eliminating every second of them.

Under closer look it occurs that there are at least three basic methods of subdividing unit length (unit square) into fractal structures of regular generalized Cantor set (or regular generalized Sierpinski carpet). It can be clear when we closer examine the simplest cases.

Let us focus on number m of closed segments in initial step of constructing regular generalized Cantor set.

If $m = 1$ we have two essential cases for number of possible divisions of I into k equal segments to get the 1D fractal generators: $k = 2$ or $k = 3$.

I. When $(m, k) = (1, 2)$ we have two segments within I. We chose one of them and eliminate entirely its interior. Without lost of generalization let us eliminate an open subset forming first half of I.

As a result there are two closed subsets left:

The point {0} being the border of eliminated open set (0, 1/2) and the other half of I, i.e. [1/2, 1]. Repeating the procedure for increasing to infinity subsequent orders r, we obtain the resulting fractal, which consists of points {0, 1/2, 3/4, …, 1}, i.e. all points $(2^n\text{-}1)/2^n$, where n is any natural number such that $n \leq r$. The point {1} is also in this set, because it includes the closed segment $[lim_{n->inf}(2^n\text{-}1)/2^n,1] = [1, 1] = \{1\}$. It means that this fractal consists of countable subset of [0,1].

II. When $(m,k) = (1,3)$ we have three equal segments within I. We chose the first and third of them and eliminate entirely their interiors. As a result there are three closed subsets left:

The point {0} and the point {1} being the borders of eliminated open sets (0, 1/3) and (2/3, 1) and the remaining third part of I, i.e. [1/3, 2/3]. The resulting fractal consists of points {0, 1/3, 4/9, 13/27, …, 1/2, …,14/27, 5/9, 2/3, 1}, i.e. all points

$(3^n/2–1/2)/3^n$, $(3^n/2 + 1/2)/3^n$, where n is any natural number such that $n \leq r$. The point {1/2} is also in this set, because it includes the closed segment $[lim_{n->inf}(3^n\text{-}1)/(2{\cdot}3^n)$, $lim_{n->inf}(3^n+1)/(2{\cdot}3^n)] = [lim_{n->inf}(1/2–1/(2{\cdot}3^n))$,

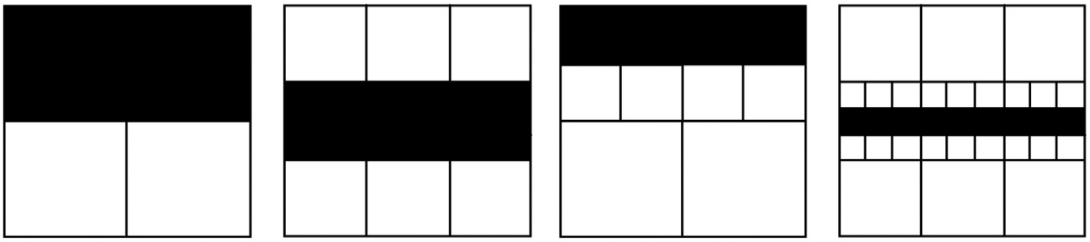

Fig. 3. Two different regular generalized Sierpinski fractals representations of first rank ($m = 1$), corresponding to the generators (a) and (b) and first following order $r = 1$ of the procedure of their generation, respectfully (c) and (d), and to different k: (a) $k = 2$, (b) $k = 3$, (c) $k = 2$ (d) $k = 3$.

$lim_{n->inf}(1/2 + 1/(2{\cdot}3^n))] = [1/2,1/2] = \{1/2\}$. It means that this fractal also consists of countable subset of [0,1].

In both above cases, the fractal dimension is 0. The number m determines the rank $m = 1$ of the corresponding regular generalized Sierpinski fractal. Both of the latter have fractal dimension equal to 1. The two pairs of numbers (m, k), i.e. (1, 2) and (1, 3), determine also the two corresponding different regular generalized Sierpinski fractals of rank m. Their zero order generators and the resulting first order $r = 1$ representations were presented at Fig. 3. Graph (c) is a result of applying twice reduced graph (a) to both upper squares of the same graph (a), and graph (d) is a result of applying triple reduced graph (b) to three central squares of the same graph (b).

In the case of $m = 1$ and $k = 1$ we would consider also trivial case of uniformly black square. In a specific way it may be treated as a result of trivial fractal generation, in which "fractal" and its trivial generator are the same objects. That is why it was not depicted in the Fig. 3 as the first case (for $k = 1$). As we see, for $m \geq 1$ we have three essential cases for the number of possible divisions of I into k equal segments: $k = 2m$-1, $k = 2$ m and $k = 2m$+1. They form generators of regular generalized Sierpinski fractals, i.e. their graphical representations of first order ($r = 1$). We will denote them as $c_{k,m}$.

For example, we have $k = 3, 4, 5$ for $m = 2$ and $k = 5, 6, 7$ for $m = 3$ (Fig. 4).

They are represented by vertical sections of diagrams from Fig. 4. Their fractal dimensions are, respectively: log m / log(2m-1), log m / log(2 m) and log m / log(2m + 1). They form three main different classes of regular generalised Cantor sets with different fractal dimensions. The fractal dimension is defined here as $D_S = \log a / \log(1/\sigma)$, where σ is a scale factor and a – the number of elements in rescaled step [3]. In our case $\sigma = 1/k$.

Fig. 4 presents the three main different classes of fractals with Sierpinski fractals representations of different type $s = (m,k)$, where $m = 2$ for different k: (a) $k = 3$, (b) $k = 4$, (c) $k = 5$; and $m = 3$ for different k: (d) $k = 5$, (e) $k = 6$, (f) $k = 7$.

To obtain the fractal dimensions of their corresponding regular generalized Sierpinski fractals one should increase them by number 1, as at this transition we have $a \to ka$, and it means that $D_S \to D_S = \log(ka) / \log(k) = 1 + \log(a) / \log(k)$.

The vertical sections of diagrams from Fig. 4 represent also three main different classes of regular generalized Cantor sets, which we denote with appropriately indexed capital letters C, i.e. as $C_{k,m}$.

In other words, linear fractal lattice $c_{k,m}$ has the fractal dimension equal to the sum of 1 and the fractal dimension of corresponding regular generalized Cantor set $C_{k,m}$.

The resulted generalized Sierpinski fractals are composed of sets of parallel sections of unit length. By repeating them along the directions of these sections we obtain lattices composed of parallel segments multiplying the initial unit length by N. We can see that only by repeating the cases (b) and (e) M times also in orthogonal direction we can cover with them the rectangle of plane of surface NxM in a regular equidistance way, forming uniformly distributed grating. In such a way, any elementary square of obtained this way NxM overlay lattice composed of them, which we can denote as $c_{k,m}^{N,M}$, will be exact copy of the same generalized Sierpinski fractal. (The other considered cases need to assume translations on other, suitably adapted steps.) That is why the second solution with even k was finally chosen. Actually, this is also the reason why $k = 16$ was used to get the fractal grating for $m = 8$ of Fig. 2. Accidentally it is equivalent there with its Sierpinski carpet, i.e. $c_{16,8} = c_{16,8}^{1,1}$. For convenience, and for avoidance of misunderstandings, as the name 'carpet' is traditionally reserved for Sierpinski fractal, we will refer to 'overlays' or 'coverlets' here, rather, as better depicting the 2D lattices composed of such carpets.

We can also generalize some of the above three subclasses key properties. If we denote $C_{k,m}$ to be an element of a subclass of regular generalized Cantor sets on $I = [0,1]$, then there exists corresponding to it regular generalized Sierpinski carpet $c_{k,m}$ on I x I, such that there exists a pair (m,k) of natural numbers $m < k$, for which

(1) $Pc_{k,m} = C_{k,m}$, where P: I x I → I is projection operator, which projects all the points contained in I x I square onto unit segment I, and
(2) there exists a reverse operation $c_{k,m} = P^{-1}C_{k,m}$, such that P^{-1}: I → I x I, and for every $y \in$ I: $(x,y) \in c_{k,m} \Leftrightarrow x \in C_{k,m}$.

The presented above example of construction of fractal grating may be more precisely discussed on an example of 1st class as follows: Let us consider a segment of unit length $\delta_d^{(o)} = n\delta_d^{(1)}$, where $n = 2d+1$, and $d = 0, 1, 2, \ldots$. Divide it into n equal parts and delete every even part of it. As a result we delete d such parts. In the second step, let us repeat the same with every undeleted segment left of length $\delta_d^{(1)} = n\delta_d^{(2)}$. In this way, at r-th step we obtain r-level set $C_d^{(r)}$ of sub-segments of equal length $\delta_d^{(r)}$ spanned within all the segments of $(r-1)$-level set $C_d^{(r-1)}$ of sub-segments of length $\delta_d^{(r-1)} = n\delta_d^{(r)}$. The number of all these r-level sub-segments from the set $C_d^{(r)}$ is $(d + 1)$ times greater than the number of all $(r-1)$-level segments from the set $C_d^{(r-1)}$.

For a specific d and r we define the *r-level subgrating* $c_d^{(r)}$ of the grating $c_d^{(r-1)}$ as the set of all strip lines (of definite width) generated by all sub-segments existing at the r-th step of the above construction as follows:

$$(x, y) \in c_d^{(r)} \Leftrightarrow x \in C_d^{(r)} \tag{2}$$

In this way we obtain r-level subgrating composed exclusively of fringes of $\delta_d^{(r)}$ width, each "compact" group $m=d+1$ of them spanned within every fringe of width $\delta_d^{(r-1)} = n\delta_d^{(r)}$ of previous stage $(r-1)$-level subgrating and each such a group of m laying in a distance $\delta_d^{(r-1)}$ from its another exact copy (the space between such a copies form blank strip of width $\delta_d^{(r-1)}$).

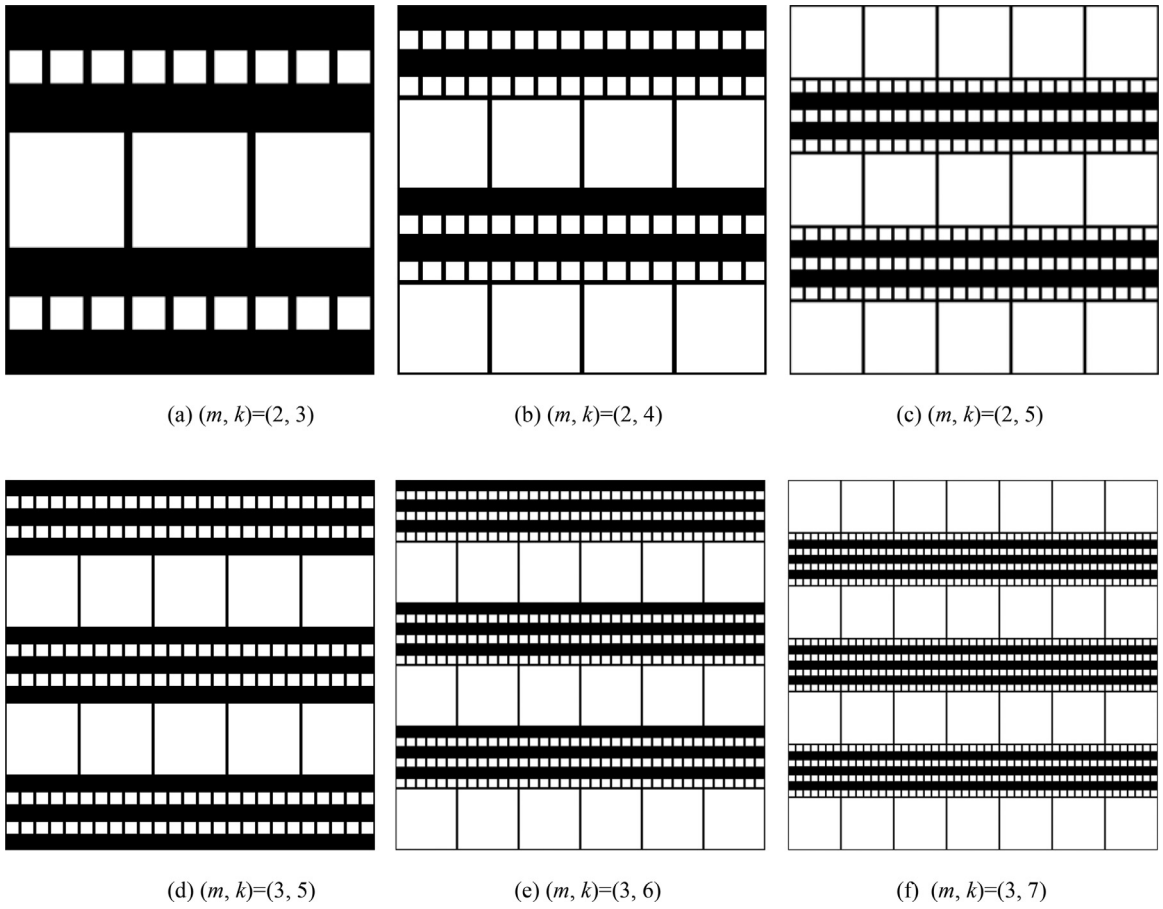

Fig. 4. Three variants of considered linear fractal gratings' generators for two-line (a, b, c) and three-line fringes (d, e, f).

It can be easily seen that the pitch within every such a group of n neighbouring fringes of $c_d^{(r)}$ – subgrating equals to $p_r = 2\delta_d^{(o)} / n^r$.

At an infinite step r for $d = 1$ as a limit of set $C_d^{(r)}$ of segments we obtain the familiar Cantor set (we denote it as C_1 - set). For $d>1$ we obtain some modified subclasses of equally familiar generalized Cantor sets [4–5]. We denote them as C_d - sets and we will call them *regular generalized Cantor sets* here. Now, we adopt these 1D C_d - sets for construction of corresponding 2D *fractal gratings* $c_{d,}$ just by setting:

$$(x, y) \in c_d \Leftrightarrow x \in C_d \tag{3}$$

We can define *finite fractal grating* by imposing the following additional criterion onto x and y: $x \in A$ and $y \in B$, where A and B are closed segments. Without lost of generalization, to stay in exact agreement with general construction of Cantor sets we will also assume here that the length of segment A is $n\delta_0 = 1$.

Suggestion of use of regular generalized Cantor sets for construction of fractal gratings is only matter of convention.

Moreover, even using regular fractal gratings, but applied to measure curvature of not in general plane surfaces, we may obtain in general non-regular moiré interference fringe patterns. Their local sections along any (straight) line in the direction perpendicular to the fringes cannot be described in general as generalized Cantor sets. This is result of the fact that for any subsequent sub-grating we may obtain different proportions (without unique transformation common for all the stages) of the set of sections used to generate generalized Cantor set.

Therefore, the fractal geometry of 2D gratings, based on regular general Cantor sets, enables derivation of moiré fringes with some deformed geometry induced by the fractal geometry of these gratings. We will refer to such a moiré fringes patterns also as fractal moiré fringes geometry. But we should remember that the fractal structure of the moiré fringes for curved surfaces is preserved only in a course manner. In general, it occurs to be more or less slightly deformed from one level to the another. It should be stressed that despite of the non-strong mathematical character of such in general differently deformed at any level overall structure, this fractal moiré fringes geometry seems to be much closer to physical fractals of real world, than accurately mathematically described fractal gratings. We can also say, that the curvature of investigated surface modulates the fractal character of moiré fringes. And only under condition that this surface is smooth enough, it can preserve the overall structure of ideal fractal geometry which we can obtain for plain surfaces.

In other words, we can say that we have to do here with passing from mathematical to physical world of fractals, as a result of adapting mathematical m-level sub-gratings to physical surfaces. We can refer to such structures as to '*weak fractals*' and we have to distinguish them from the common '*strong fractals*', for which we can give a strong mathematical rule for deformation between subsequent levels, common for all these levels.

For example, when we stay at the level of mathematical reality, and use mathematical continuous smooth-enough surfaces we can easily obtain locally strong fractal moiré fringes geometry starting from some high enough r-level sub-grating, for which the curvature of the surface may be neglected. However, up to that r-level we are forced to treat this structure (globally) as a weak fractal.

5. Fractal moiré fringe patterns

The mentioned in the Introduction, well known methods of projecting two or more gratings onto the surface of different objects for needs of geometrical moiré techniques [2] should be clearly distinguished from the method of applying fractal gratings discussed here.

The resulting pattern of moiré fringes of the second order (which may be observed at the area of overlapping of the lines of lower order - the dark vertical lines) mirrors the rougher pattern of moiré fringes of the first order. It does mean that the fine structure of the intersecting lines of the second order, when magnified, gives the same general picture as the one presented in the Fig. 2, if only we make them to be subdivided into m subsequent lines of the 3rd order.

In such a way, the fractal structure of moiré fringes may be obtained, with every light (this is not mistake!) fringe composed of these finer dark moiré fringes of the subsequent order, chopped with vast clear areas. When smooth enough, these fine fringes may be easily interpolated for achieving their continuity. They may be properly distinguished and, in consequence, interpreted also while depicting the surface roughness of comparable extension. It does mean that the method may occur to be particularly suitable for depicting the roughness of surfaces having fractal character itself. The suitable fractal grating may be applied then for measurements of such fractal surfaces for obtaining the best possible adjustment.

However, the question of maximal usable fractal order arises, especially while considering the typical optical setups. It need to be clearly stated that the pure mathematical strong fractals are not present in nature. And only their finite iterations referred above as weak fractals are present in it, as they are restricted there by finite dimensions of atoms and chemical particles. In a similar way only first few finite steps of fractal gratings will have practical significance. In particular, when measuring some geometrical properties of physical objects we are restricted by their quantum nature. Therefore, this means that in Nature, we generally need restrict ourselves only to some finite approximations of such mathematical entities as both points and lines, but also the fractals. However, to obtain strong mathematical description, we use these idealized mathematical tools for needs of generalization, applicable to as many levels of physical realm as possible, and in possible universal form.

In the case of fractal gratings the lower limits are determined by general limitations of optical measurement methods, and the later are restricted by limitations resulted from light wavelength used. As the interference (fringe pattern) methods allow measurements down to atomic scale, e.g., at X-ray range [6] or in a scanning transmission electron microscope (STEM) Moiré interferometry [7], we may expect that the proposed method may find application in such fields when we need to control processes demanding distinguishing between, e.g., molecular level and atomic level structures, or between nanostructures' and microstructures' levels; including different scale of crystalline structures faults. These applications will be restricted only with light, X-ray or electrons of specific wavelength ability to resolve two lines of following rank of fractal grating.

While analysing resulting interference patterns, we may try to record at least two neighbouring levels of resulting fringe patterns. However, when the former is not possible, we may still technically restrict to record and analyse the courser or finer images, separately. Why placing camera far enough away to take whole the global picture (with lower resolution) or closer to take the chosen part (local parts) of the moiré fringes picture (with higher resolution). An advantage of this method is therefore that, that we can apply/attach a single grid to the object surface and get both fine (local) and rough (global) results with it, not only in short but also after longer periods between following measurements. (And only in the case of some lower order gratings the camera will be able to resolve two following ranks while placing in mid-way.) Using such a grating will led to exactly the same troubles with resolution of camera placed at some remote enough distance from the object surface, as it takes place in the case of common gratings with uniformly distributed line patterns. When the pitch is too small, instead of getting the global interference, the camera would record merely a uniformly grey object plane, unable to resolve the dense grating lines. And when camera is too close, we would record only few lines without significance. However, in the case of fractal gratings, it could mean that in practice we can use even three- or four-level fractal subgratings with a single camera moving still closer to the tested surface, to get up to four sets of still more local interference patterns, when needed. Moreover, with a very precise fractal grating, and applying cameras of greater resolution (e.g. microscope), we are restricted only with technical precision of preparing fractal grating and a set of optical instruments of increasing optical resolution. Alternatively, we may manipulate with the general rank m of such fractal grating structure, accordingly on the stage of measurement experiment designing, and providing the best suitable fractal grating of m-lines fringes, where needed. Adjusting not only grating pitch p parameter, but also number m of following sublines in a single fractal grating "line" to the true fractal dimension of tested fractal-like structure.

Also the angle β between interfering gratings (model one and the reference one) can serve as the third parameter allowing optimal analysis of tested object deformation.

The angle γ of fringe inclination in relation to lines of one of the gratings is determined from the symmetry of the problem: moiré fringes lie along the direction of bisector of obtuse angle between lines of interfering gratings. For $\beta = 10^\circ$ we have for every interference case at common plane from Fig. 2 $\gamma = 85^\circ$ and w is determined from Eq. (1) as $w = 5.7369\ p_0$.

When we replace pitch of starting gratings p_0 with a pitch p_r of r-level subgrating, we obtain the value $w^{(r)} = 5.7369\ p_r$ for the distance of these finer fringes for any r-level subgrating. For interference in common plane, the structure of fringes for the r-level subgratings mirrors exactly the structure for $(r\text{-}1)$-level subgrating with the scale factor $w^{(r-1)} / w^{(r)} = p_{r-1} / p_r = 2m$, where m is number of lines into which we split every line of lower level subgrating.

The rough level of the fractal grating pattern may be used for obtaining fringe patterns mapping the overall deformation of surfaces of different technical objects while the subtle pattern can be used to map deformations of details of these surfaces by applying the model (specimen) fractal gratings to these objects' surfaces. The general fractal pattern properties can be applied with the demanded for convenient needs number of first rank rough lines, each of which is composed of m sub-lines. The fractal subsequent sub-lines which can be divided into m sub-sub-lines in the second step, and so on, are represented by continuous lines approximating this fractal grating, according to the needs of the assumed target application. The fringe pattern obtained with the use of reference (master) grating, being, e.g., the grating composed of lines of pixels of computer monitor screen, may be used to get the moiré pattern of the first (rough) fractal grating rank. This can be analysed in a usual numerical way presented, e.g., at works [8] and [9].

The subtle fractal structure can be obtained both with reference fractal grating or common master grating type from Fig. 1**a** of close lines density (or the grating pitch) close to the lines density of the second (subtle) order of the applied fractal grating type from Fig. 2**a** placed in the direct vicinity of analysed surface detail area. It can be analysed digitally for each particular rough bar composed of m subtle lines in a way described, e.g., in [10], i.e. by searching the best correlation with 2D periodic analytical function,

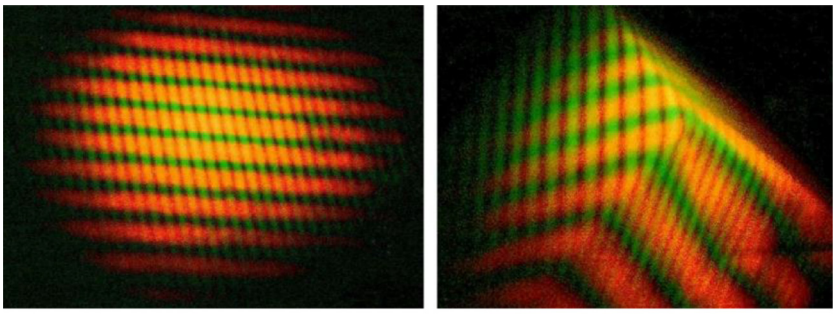

Fig. 5. An example of two sets of coloured fringes projected with the use of double laser intereferometer onto different test surfaces: flat (a) and cubical (b).

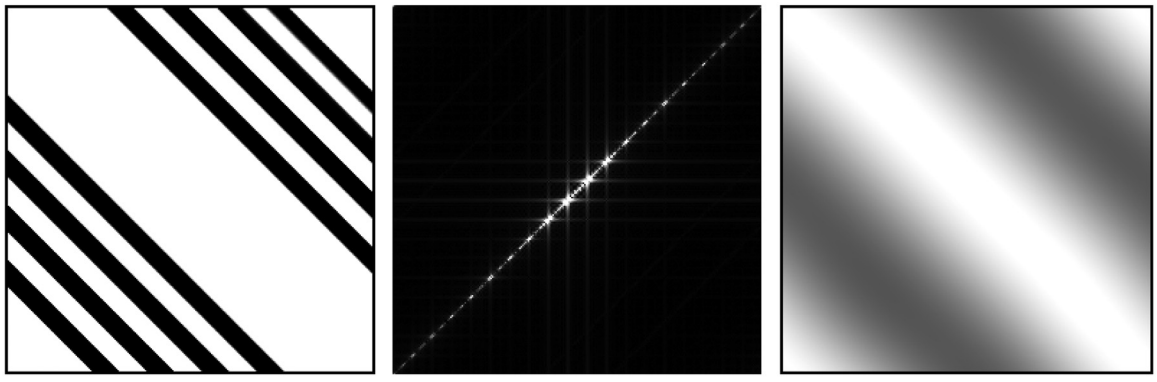

Fig. 6. An example of the part of $c_{4,7}$ fractal graphical representation (a) with its 256 × 256 point FFT (b), and reverse FFT of only tiny central part of the former of 5 point diameter (c).

and then with the possible further applying of analytical interpolation between functions for neighbouring bars composed of m lines each. The obtained functions will represent the 2D map of local deformations of applied to the tested surface fractal grating and can be used to verify the degree of precision of the specimen grating adhering to the object surface.

An alternative of two-colour composed fractal lattice with the blank rough lines replaced with the other colour copy of subtle structure of rough dark lines can be also applied to avoid necessity of applying non-unique analytical interpolation. Such an approach will be proposed in developed separate future article developing the idea of two-coloured fractal moiré grating based on a suitably generalized idea of double laser interferometer [8,9] with two colour groups of fringes projected on an object surface and subsequently analysed separately after colour digital filtration (Fig. 5). The latter is a particular case of more general Polychromatic Light Interferometry [11] and Variable Wavelength Interferometry [12]. Alternatively, two different-colour mutually orthogonal fractal gratings may be used in exactly the same manner as two different-colour common fringe gratings were used at Fig. 5.

Often the Fourier techniques are used to analyse the interference patterns. 2D Fourier Transform is particularly suitable when we need to filter-out the higher frequencies from an image to perform automatic delineation of recorded fringes to analyse them with computer means [13]. Fig. 6 presents the case of part of graphical representation of $c_{4,7}$ fractal with its 256 × 256 point FFT and reverse FFT of only tiny central part of the former of 5 point diameter. All the other points of FFT were filtered out by assuming all of them equal to 0. As result we obtain only its lower level graphical representation with additionally smoothened lines. Their subtle structure was filtered out.

Another examples present the same case of fractal $c_{4,7,}$ however, with three level graphical representation. It means that the dark lines from Fig. 6 were subdivided into four lines of following subtle structure, each. For convenience the angle of their presentation was changed from 45° to horizontal layout.

Fig. 7 presents the case of part of graphical representation of $c_{4,7}$ fractal with its 256 × 256 point FFT and reverse FFT of only 60 × 60 points central part square of the former. All the other points of FFT were filtered out by assuming all of them equal to 0. As result we obtain only its lower level graphical representation with additionally smoothened lines. Their subtle structure was filtered out.

Fig. 8 presents the same case of part of graphical representation of $c_{4,7}$ fractal with its 256 × 256 point FFT and reverse FFT of only 12 × 12 points central part square of the former. All the other points of FFT were filtered out by assuming all of them equal to 0. As result we obtain only its lowest level of graphical representation with additionally smoothened lines. The two following subtle structure levels were filtered out.

The above procedure of applying FFT filtration to true fractal lattice (two-level or three-level as considered above) enable quantity analyses of more rough (lower level) fringe structures in usual way, i.e. by their delineation of fringes at wanted level of mapping of surface details, of fractal character itself. It can be directly applied particularly for mapping surfaces of fractal character by the method of optical projection of such finite (few first step only) graphical representations of fractal fringe structure on analysed surface.

Moreover, while analysing resulting interference patterns, we prevailingly need technically restrict to record and analyse the courser or finer images, separately. Why placing camera far enough away to take whole the picture (with lower resolution) or closer

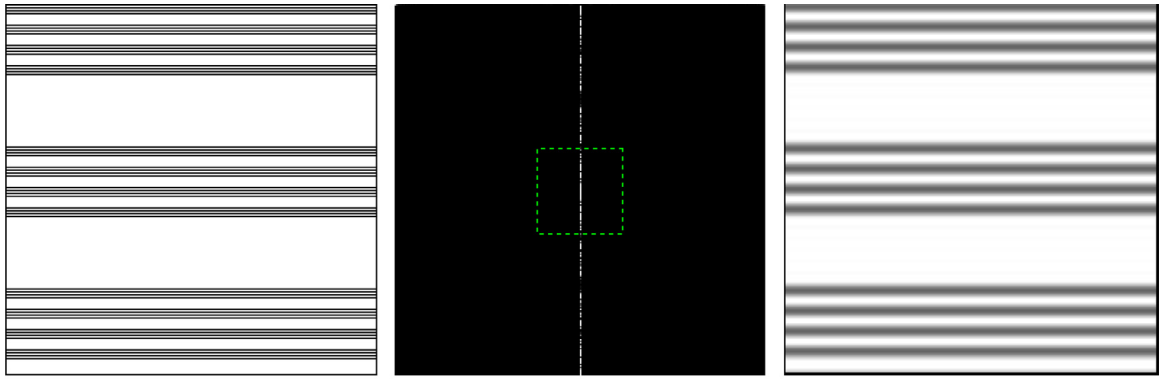

Fig. 7. An example of the part of $c_{4,7}$ fractal graphical representation (a) with its 256 × 256 point FFT (b), and reverse FFT of only 60 point side central square part of the former (c).

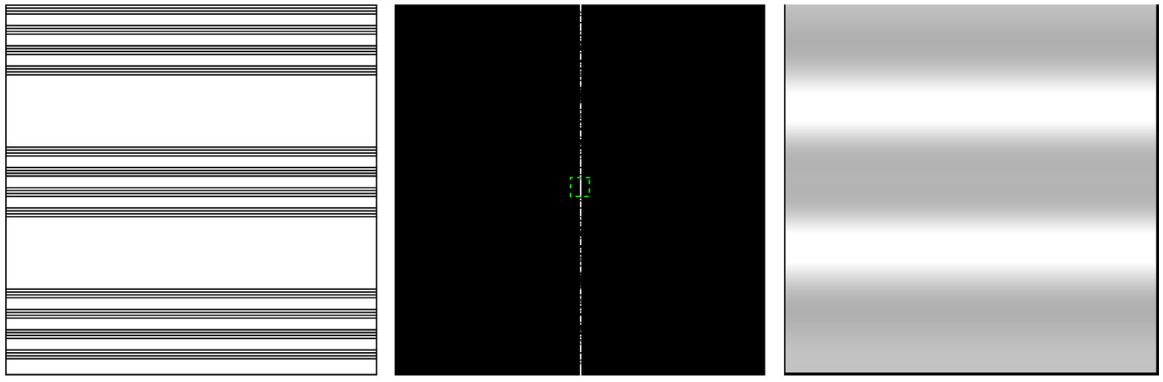

Fig. 8. An example of the part of $c_{4,7}$ fractal graphical representation (a) with its 256 × 256 point FFT (b), and reverse FFT of only 12 point side central square part of the former (c).

to take the chosen part (parts) of the picture (with higher resolution). An advantage of this method is that we can apply/attach a single grid to the object surface and get both fine (local) and rough (global) results with it. Both in short, as well as longer periods between following measurements. As there was discussed here only one of two colour components needed to manage with empty spaces, it should be indicated once more on the two-colour solution as providing the data possible to get also with uniform dense grating. However, using such a grating will led to the troubles with resolution of black & white camera placed at some remote enough distance from the object surface, as why we would try to get the global interference, the camera would record merely a uniformly grey object plane, unable to resolve the dense grating lines. That is precisely when the more rough strip structure of fractal grating will demonstrate its advantages. The problem may be also solved by applying colour camera with following filtering, or, alternatively using one or two black&white cameras with different optical filters.

6. Conclusions

The new FMI (Fractal Moiré Interferometry) method, presented above, may be used for obtaining better results in mapping surfaces of different physical objects during their dynamical changes, beginning from various industrial devices, through objects in micro and nano-scale, up to multilayered crystalline structures faults. In particular, simultaneous recording of two different size components of deformations with two different levels of resolution, may be especially suitable for determining comparatively large-range changes in object's surface resulting in, e.g., simultaneous rough and fine deformations under static load or many-harmonic excited vibrations. It may be alternatively used for determining rough deformations of large plane surfaces, such as, e.g., present in road/rail noise barriers, and also detecting of small deformations responsible for wrong attachments of model (specimen) grating to measured surface.

As the resulting subsequent fringe patterns form the usual fringe patterns only in the areas of overlapping of more rough lines, it may occur to be necessary to scan the specimen grating with the master one in a suitable manner. To achieve this the master grating should be simply moved in the primary direction on a half pitch of the first order grating. Alternatively, the colour master grating could be applied. In the case of specimen grating bonded to the investigated surface, effectively, only half of the surface (in the area covered with the rougher lines) may be investigated for the finer effect by the scanning method. That is why the proposed method is most suitable for projected (shadow) moiré interferometry. The further developing of presented here idea to the form of two-coloured fractal moiré lattices will be most likely necessary to avoid non-unique analytical interpolation, may occur to be more convenient in similar future applications. The potential usefulness of application of Fourier Trans-

form methods for extracting fringes of particular fractal lattice level may also need further investigations. The entirely new wide field of extension of known optical interference methods by applying fractal gratings to the already existing and widely used measurement methods in physics was born, which provides them with more subtle analytical tool for effective simultaneous dynamical research on many-level fractal-like phenomena we are observing in nature.

CRediT authorship contribution statement

Zbigniew Motyka: Conceptualization, Methodology, Software, Validation, Data curation, Formal analysis, Investigation, Writing – original draft, Visualization, Writing – review & editing.

Acknowledgments

Work was led within part of activities of Central Mining Institute (Główny Instytut Górnictwa), Katowice, Poland (which provided necessary Resources), within International (with participation of Austria, Cyprus, Poland and Spain) Project CEFRABID (Project number: SOLAR-ERA.NET Cofund 1 N° 043. Project www page: http://cefrabid.gig.eu/en/node/41), which was supported under the umbrella of SOLAR-ERA.NET Cofund by FFG in Austria, RPF in Cyprus, NCBR in Poland and MINECO-AEI in Spain. SOLAR-ERA.NET is supported by the European Commission within the EU Framework Programme for Research and Innovation HORIZON 2020 (Cofund ERA-NET Action, N 691664).

CEFRABID supervision and administration 2018–2020 (Management and coordination responsibility for the CEFRABID project research activity planning and execution): Zbigniew Motyka, GIG. Funding (in Polish part financed by the National Centre for Research and Development NCBR, Poland, under the Agreement No. SOLAR/01/CEFRABID/2018).

References

[1] Khan AS, Wang X. Strain measurements and stress analysis. New Jersey: Prentice Hall; 2001.
[2] Groves RM, James SW, Tatam RP. Shadow Moire method for the determination of the source position in three-dimensional shearography. Opt Lasers Eng 2001;36:317–29.
[3] Peitgen HO, Jurgens H, Saupe D. Fractals for the classroom, part 1: introduction to fractals and chaos. Springer-Verlag New York, Inc; 1992.
[4] Hutchinson JE. Fractals and self similarity. Indiana Univ Math J 1981;30:713–47.
[5] David G, Semmes S. *Fractured fractals and broken dreams*, oxford lecture series in mathematics and its applications, 7. Oxford: Clarendon Press; 1997.
[6] Stein AF, Ilavsky J, Kopace R, Bennett EE, Wen H. Selective imaging of nano–particle contrast agents by a single-shot X-ray diffraction technique. Opt Express 2010;18(12):13271–8.
[7] Pofelski A, Woo SY, Le BH, Liu X, Zhao S, Mi Z, Löffler S, Botton GA. 2D strain mapping using scanning transmission electron microscopy Moiré interferometry and geometrical phase analysis. Ultramicroscopy 2018;187:1–12.
[8] Motyka Z. Double integrated laser interferometer. Proceeding of SPIE. 5229, laser technology VII: applications of lasers; 2003.
[9] Motyka Z, Passia H. Dual integrated laser interferometer for fringe projection techniques. In: Tomasini Enrico Primo, editor. AIP conference proceeding, 1457. America Institute of Physics; 2012. p. 451. https://www.gig.eu/sites/default/files/attachments/zaklady/seminarium05082012zm_hp_aivela.pdf.
[10] Aloszko S, Motyka Z, Passia H. Interferometric holography of thin rods and coal beds. Proceeding SPIE. 859, laser technology II; 1987.
[11] Dobosz M, Matsumoto Hirokazu, Seta Katuo, Iwasaki Shigeo. Polychromatic light interferometer for high-accuracy positioning. Opt Lasers Eng 1996;24:43–56.
[12] Pluta M. Variable wavelength microinterferometry of textile fibres. J Microsc 1988;149:97–115.
[13] Motyka Z. Podwójny interferometr laserowy do ilościowej analizy kształtu i deformacji powierzchni technicznych obiektów przemysłowych (Dual laser interferometer for the quantitative analysis of the shape and deformation of technical surfaces of industrial facilities). Wiad Górnic 2005;5:245–53.